JOURNAL OF MATERIALS SCIENCE **36** (2001) 2095–2104

New analysis on the fiber push-out problem with interface roughness and thermal residual stresses

YOUNG S. CHAI*, YIU-WING MAI‡
Centre for Advanced Materials Technology (CAMT), Department of Mechanical and Mechatronic Engineering J07, The University of Sydney, Sydney, NSW 2006, Australia
E-mail: mai@mech.eng.usyd.edu.au

An improved analysis considering the effects of interface roughness and thermal residual stresses in both radial and axial directions is developed for the single fiber push-out test. The roughness of the interface, which has a significant effect on the fiber sliding behavior, is expressed by a Fourier series expansion that has good convergence and can handle general shapes of roughness. The interfacial shear stress that plays an important role in interfacial debonding is very much affected by the axial thermal residual stress in the bonded region, which can induce a two-way debonding mechanism. It has been found that both residual stress and interface roughness have pronounced effects on the stress transfer across the interface and interfacial debonding behaviour.

1. Introduction

Structural reliability of composite materials can be strongly affected by the fracture properties of the interface between fiber and matrix [1, 2]. Recently, there is much interest on the debonding phenomenon and frictional sliding behaviour along composite interfaces. An important feature in fibrous composite applications to engineering technology is the stress transfer between fiber and matrix across the interface. Along the perfectly bonded region, the elastic stress transfer at the interface can be determined. Apart from this, another important phenomenon in brittle matrix composites is the stress transfer by friction governed by Coulomb's friction law after the interface bond has failed. The load-bearing capacity of composite materials depends on the efficiency of stress transfer at the bonded and debonded interfaces, which are mainly controlled by the mechanical properties of fiber and matrix and by the nature of the bonding.

It is reported that interface frictional sliding of fibers is a major toughening mechanism that occurs in the crack-wake bridging zone [1–3]. Progressive debonding and frictional sliding at the interface are hence of fundamental interest. Single fiber pull-out and/or push-out techniques have been used to characterize the behavior of the interface between these two constituents. Initial and maximum debond stresses as well as frictional pull-out and/or push-out stresses can be determined from experimental load-displacement curves. Analyses have also been developed for the test to provide a theoretical basis for experimental determination of the interfacial properties [4–6]. Although most of the previous models do not include the roughness of the debonded interface that has a pronounced effect on the interfacial frictional sliding behavior, some recent studies have indeed considered this effect analytically and/or experimentally.

When a single fiber is pulled and/or pushed, a push-back phenomenon that results in a 'reseating load drop' was first reported by Jero and Kerans [7] for fiber push-out. This result has also been confirmed by Carter *et al*. [8] using a fiber pull-out test. The observation of a fiber being pushed back to the original position indicated directly that the fiber and the matrix have a rough interface in the debonded region. Kerans and Parthasarathy [9] included the effects of interface roughness and residual axial strain in the fiber to predict the load-displacement behavior. Their model is expected to be appropriate for relatively large sliding displacements. However, in many crack-bridging problems, the sliding displacements are small. Therefore, their analyses are extended to include effects of interfacial roughness by introducing a friction parameter [10]. They also studied the effect of interfacial roughness on the frictional sliding using fiber push-out and push-back tests on a model composite of Plexiglas rods in an epoxy matrix [11]. Mackin *et al*. [12, 13] have developed an analytical model of fiber sliding for the push-out problem. The roughness of the debonded interface was modeled using fractal algorithms with identical fractal profiles assigned to both sides of the debond, but the effects of the axial elastic deformations of both fiber and matrix to the asperity mismatch were neglected for the full fiber sliding process. Liu *et al*. [14] have given a more rigorous

* *Present Address*: School of Mechanical Engineering, Yeungnam University, Gyongsan 712-749, Korea.
‡ *Present Address*: Department of Manufacturing Engineering and Engineering Management, City University of Hong Kong, Tat Chee Avenue, Kowloon, Hong Kong.

model for a single fiber pull-out with a rough interface using a Fourier series approach. It was assumed that the interface between fiber and matrix has been completely debonded and the solutions of fiber pull-out stress and relative displacement along the interface were derived. They extended their analysis to the case of fiber push-out in terms of asperity wear to simulate the change of the frictional push-out stress during fiber sliding [15]. The advantage of the Fourier representation, as distinct from earlier studies, is that it can accommodate many different surface roughness profiles. Also, a recent model of an interface with micro-dilatancy was proposed by Stupkiewicz [16] in which the radial misfit varies and depends on the relative displacement by extending the model of a strip on a frictional foundation. The irreversible effects of wear of asperities can be included for large sliding distances or for cyclic loading. Parthasarathy and Kerans [17] studied the potential effects of interfacial roughness in ceramic composites using a model that included the progressively increasing contribution of roughness.

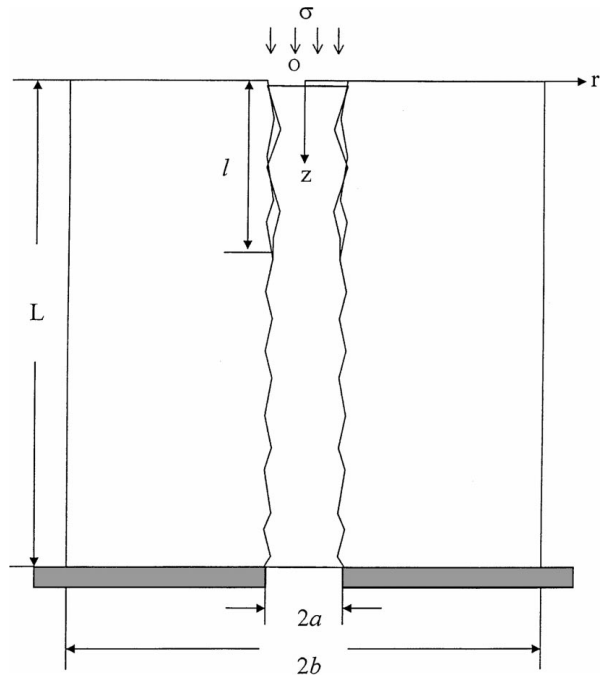

Figure 1 Schematics of the model for single fiber push-out.

2. The present work

The present paper describes an improved single fiber push-out model in consideration of interface roughness and thermal residual stresses in both radial and axial directions. Most of the existing analyses considered the thermal residual stress in the radial direction that arises from mismatch of the coefficients of thermal expansion between the two constituents along the interface. While previous studies [9, 10, 16, 17] have included models with interface roughness and thermal residual stresses in both directions, relatively little effort seems to have been spent to explain the significant effect of the thermal residual stress in the axial direction on the stress distribution in the bonded region. The interface between fiber and matrix is initially perfectly bonded, then partially debonded, and finally completely debonded as the external load is gradually increased. In comparison with earlier investigations [14, 15], a full range of loading and interfacial bond conditions were considered in this paper in order to characterize the debonding and frictional sliding behaviours during the evolution of the whole fiber push-out process.

Shear-lag models were used to model the fiber-matrix system and to determine interface properties. The interface roughness was expressed by a Fourier series expansion that had good convergence and could handle general shapes of roughness as mentioned earlier. With this approach, geometric details of roughness are characterised by the average wavelength and the maximum amplitude. It is felt, however, that these two parameters are sufficient to differentiate the influences of the surface geometries as shown in [14]. The effect of the axial thermal residual stress on stress distribution in the bonded region was also rigorously considered. Effects on the axial and shear stress distributions, that is, stress transfer properties, and interfacial debonding behaviour, such as stress required for further debonding, were studied. It is concluded that the stress distributions in the bonded region are significantly affected by the presence of the thermal residual stress in the axial direction. The distribution of the interfacial shear stress in the bonded region suggests possible two-way debonding, which was rarely reported in previous work except in [18, 19]. It also confirmed that the interface roughness is an important cause of crack toughening. Therefore, both thermal residual stresses and interface roughness had pronounced effects on the stress transfer across the composite interface and the interfacial debonding behaviour.

3. Theoretical analysis

The geometry of a composite cylindrical model for single fiber push-out test is shown in Fig. 1. A set of cylindrical coordinates (r, θ, z) is selected such that the z-axis corresponds to the axis of the fiber and r is the distance from the fiber axis. L is the whole embedded axial length, and from which l is the debonded length. A fiber of radius a is located in the center of the matrix shell of radius b. The matrix is fixed at the bottom end $(z = L)$ and a compressive stress, σ, is applied to the fiber end $(z = 0)$. The mode of deformation is axisymmetric and the stress and displacement components are all independent of the circumferential direction θ. It is assumed that the axial stress components in both the fiber and matrix are independent of the radial coordinate as in previous studies [14, 15].

3.1. Basic equations ($0 < z < L$)

The equilibrium equations of fiber, matrix and interface by taking compressive stress as positive require that:

$$\sigma_f^z(z) + \frac{1}{\gamma}\sigma_m^z(z) = \sigma \tag{1}$$

$$\frac{d\sigma_f^z(z)}{dz} = -\frac{1}{\gamma}\frac{d\sigma_m^z(z)}{dz} = -\frac{2}{a}\tau(z) \tag{2}$$

$$\frac{\partial\sigma_m^z(z)}{\partial z} + \frac{\partial\tau_m^{rz}(r,z)}{\partial r} + \frac{\tau_m^{rz}(r,z)}{r} = 0 \tag{3}$$

where $\gamma = \frac{a^2}{b^2-a^2}$, and $\tau(z)$ in Equation 2 is the interfacial stress which is defined as $\tau(z) = \tau_m^{rz}(a, z)$. By assuming the fiber and matrix to be isotropic, the stress-strain relationships are given by:

$$\varepsilon_f^{\theta}(r,z) = \frac{1}{E_f}\left[\sigma_f^{\theta}(r,z) - \nu_f\left\{\sigma_f^{r}(r,z) + \sigma_f^{z}(z)\right\}\right] + \alpha_f \Delta T \quad (4)$$

$$\varepsilon_f^{z}(r,z) = \frac{1}{E_f}\left[\sigma_f^{z}(z) - \nu_f\left\{\sigma_f^{r}(r,z) + \sigma_f^{\theta}(r,z)\right\}\right] + \alpha_f \Delta T \quad (5)$$

$$\varepsilon_m^{\theta}(r,z) = \frac{1}{E_m}\left[\sigma_m^{\theta}(r,z) - \nu_m\left\{\sigma_m^{r}(r,z) + \sigma_m^{z}(z)\right\}\right] + \alpha_m \Delta T \quad (6)$$

$$\varepsilon_m^{z}(r,z) = \frac{1}{E_m}\left[\sigma_m^{z}(z) - \nu_m\left\{\sigma_m^{r}(r,z) + \sigma_m^{\theta}(r,z)\right\}\right] + \alpha_m \Delta T \quad (7)$$

From Equations 2 and 3, the shear stress distribution in the matrix $\tau_m^{rz}(r,z)$ could be expressed in terms of interfacial stress $\tau(z)$

$$\tau_m^{rz}(r,z) = \frac{\gamma(b^2 - r^2)}{ar}\tau(z) \quad (8)$$

3.2. Stresses in the debonded region ($0 < z < L$)

In the debonded region, frictional slip based on Coulomb friction law occurs along the interface. Interfacial shear stress $\tau(z)$ is governed by frictional sliding as follows

$$\tau(z) = \mu q(z) \quad (9)$$

where $q(z)$ is the interfacial radial stress (compressive) and could be represented by

$$q(z) = -[q_o - q_a(z) - q_R(z)] \quad (10)$$

where q_o is the thermal residual stress (compressive) in the radial direction. $q_a(z)$ is the term caused by the Poisson's effect and $q_R(z)$ is due to the interaction of interfacial roughness between fiber and matrix. Residual stress in the radial direction q_o can be derived by considering the continuity of circumferential strains in Equations 4 and 6 as

$$q_o = \frac{E_m(\alpha_m - \alpha_f)\Delta T}{\alpha(1-\nu_f) + (1 + 2\gamma + \nu_m)} \quad (11)$$

where $\alpha_f(\alpha_m)$ is the thermal expansion coefficient of the fiber (matrix), and ΔT is the temperature change. $q_a(z)$ due to Poisson's effect can also be obtained from

$$q_a(z) = k_1\sigma_f^{z}(z) - k_2\sigma \quad (12)$$

where

$$k_1 = \frac{\alpha\nu_f + \gamma\nu_m}{\alpha(1-\nu_f) + (1 + 2\gamma + \nu_m)} \quad (13)$$

$$k_2 = \frac{\gamma\nu_m}{\alpha(1-\nu_f) + (1 + 2\gamma + \nu_m)} \quad (14)$$

and $\alpha = \frac{E_m}{E_f}$.

Another contribution of radial stress $q_R(z)$ is due to the overlapping of the amplitude of a fiber-matrix asperities mismatch $\delta(z)$

$$q_R(z) = \frac{K}{a}\delta(z) \quad (15)$$

in which

$$K = \frac{\alpha E_f}{\alpha(1-\nu_f) + (1 + 2\gamma + \nu_m)} \quad (16)$$

The interfacial amplitude function $d(z)$ can be expressed in terms of a Fourier series:

$$d(z) = \frac{1}{2}d_o + \sum_{n=1}^{\infty} d_n \cos\frac{n\pi z}{L} \quad (17)$$

where d_n is the coefficient of the Fourier series for $d(z)$

$$d_n = \frac{2}{L}\int_0^L d(z)\cos\frac{n\pi z}{L}\,dz \quad (18)$$

The asperities mismatch function $\delta(z)$ resulting from the relative displacement of the interfaces $v(z)$ in the z-direction is given by:

$$\delta(z) = d[z - v(z)] - d(z) = \sum_{n=1}^{\infty} d_n\left[\cos\left(\frac{n\pi\{z - v(z)\}}{L}\right) - \cos\frac{n\pi z}{L}\right] \quad (19)$$

$\delta(z)$ can also be represented by a Fourier series as

$$\delta(z) = \frac{1}{2}B_o + \sum_{n=1}^{\infty} B_n \cos\frac{n\pi z}{L} \quad (20)$$

where

$$B_n = \frac{2}{L}\int_0^L \delta(z)\cos\frac{n\pi z}{L}\,dz \quad (21)$$

The differential equation for axial fiber stress is obtained by combining Equations 2, 9, and 10 as follows:

$$\frac{d\sigma_f^{z}(z)}{dz} = \frac{2\mu}{a}[q_o - q_a(z) - q_R(z)] \quad (22)$$

Inserting Equations 12, 15 and 20 into Equation 22 and with the stress boundary condition $\sigma_f^{z}(0) = \sigma$, the solution of the axial fiber stress becomes:

$$\sigma_f^{z}(z) = \sigma - \omega(\bar{\sigma} + \sigma)(1 - e^{-\lambda z}) - \frac{K}{ak_1}\sum_{n=1}^{\infty}\frac{(\lambda L)^2 B_n}{(\lambda L)^2 + (n\pi)^2} \bullet \left(\cos\frac{n\pi z}{L} + \frac{n\pi}{\lambda L}\sin\frac{n\pi z}{L} - e^{-\lambda z}\right) \quad (23)$$

where

$$\lambda = \frac{2\mu k_1}{a} \quad (24)$$

$$\omega = \frac{1}{k_1}(k_1 - k_2) \quad (25)$$

$$\bar{\sigma} = \frac{-1}{k_1 - k_2}\left(q_o - \frac{KB_o}{2a}\right) \quad (26)$$

The stress at the debond front is obtained from $\sigma_f^{z}(z)$ in Equation 23, i.e.

$$\sigma_f^l = \sigma - \omega(\bar{\sigma}+\sigma)(1-e^{-\lambda l}) - \frac{K}{ak_1}\sum_{n=1}^{\infty}\frac{(\lambda L)^2 B_n}{(\lambda L)^2+(n\pi)^2}\bullet\left(\cos\frac{n\pi l}{L}+\frac{n\pi}{\lambda L}\sin\frac{n\pi l}{L}-e^{-\lambda l}\right) \quad (27)$$

From the solution of axial fiber stress $\sigma_f^z(z)$, the corresponding matrix axial stress $\sigma_m^z(z)$ and matrix shear stress $\tau_m^{rz}(z)$ are obtained. That is,

The resulting solution of the relative displacement subjected to the boundary condition $v(l)=0$, is given by

$$\sigma_m^2(z) = \gamma\omega(\bar{\sigma}+\sigma)(1-e^{-\lambda z}) + \frac{\gamma K}{ak_1}\sum_{n=1}^{\infty}\frac{(\lambda L)^2 B_n}{(\lambda L)^2+(n\pi)^2}\bullet\left(\cos\frac{n\pi z}{L}+\frac{n\pi}{\lambda L}\sin\frac{n\pi z}{L}-e^{-\lambda z}\right) \quad (28)$$

$$\tau_m^{rz}(r,z) = \frac{\gamma(b^2-r^2)}{2r}\left\{\lambda\omega(\bar{\sigma}+\sigma)e^{-\lambda z} + \frac{K}{ak_1}\sum_{n=1}^{\infty}\frac{(\lambda L)^2 B_n}{(\lambda L)^2+(n\pi)^2}\bullet\left(-\frac{n\pi}{L}\sin\frac{n\pi z}{L}+\frac{n^2\pi^2}{\lambda L^2}\cos\frac{n\pi z}{L}+\lambda e^{-\lambda z}\right)\right\} \quad (29)$$

Initial frictional push-out stress (σ_{ifr}) at the onset of complete debonding of the fiber is determined from the condition $\sigma_f^l = 0$ when $l = L$

$$\sigma_{ifr} = \frac{1}{1-\omega(1-e^{-\lambda L})}\left\{\omega\bar{\sigma}(1-e^{-\lambda L}) + \frac{K}{ak_1}\sum_{n=1}^{\infty}\frac{(\lambda L)^2 B_n}{(\lambda L)^2+(n\pi)^2}[(-1)^n - e^{-\lambda L}]\right\} \quad (30)$$

which is equivalent to the previous result [15].

To evaluate the stress distribution, the coefficients (B_n, where $n = 0, 1, 2, \ldots \infty$) of asperity mismatch $\delta(z)$ must be determined by solving the relative displacement $v(z)$ of the fiber and matrix

$$\frac{dv(z)}{dz} = \frac{d}{dz}\left(u_f^z - u_m^z\right) = -\left(\varepsilon_f^z - \varepsilon_m^z\right) \quad (31)$$

From Equation 1, 5, and 7, Equation 31 becomes

$$\frac{dv(z)}{dz} = -\frac{1}{\alpha E_f}\left[\lambda_1\sigma_f^z(z) - \lambda_2\sigma + \lambda_3 q_R - \lambda_3 q_o + \sigma_o\right] = -\frac{1}{\alpha E_f}\left[\lambda_1\sigma_f^z(z) - \lambda_2\sigma - \lambda_3 q_o + \sigma_o + \lambda_3\frac{K}{a}\left(\frac{1}{2}B_o + \sum_{n=1}^{\infty}B_n\cos\frac{n\pi z}{L}\right)\right] \quad (32)$$

where

$$\lambda_1 = \alpha + \gamma + k_1\lambda_3 \quad (33)$$

$$\lambda_2 = \gamma + k_2\lambda_3 \quad (34)$$

$$\lambda_3 = -2(\alpha\nu_f + \gamma\nu_m) \quad (35)$$

and

$$\sigma_o = E_m(\alpha_m - \alpha_f)\Delta T \quad (36)$$

$$v(z) = \frac{1}{\alpha E_f}\left(\frac{\lambda_1 k_2 - \lambda_2 k_1}{k_1}\sigma - \omega\lambda_1\bar{\sigma} - \lambda_3 q_o + \sigma_o + \frac{\lambda_3 K B_0}{2a}\right)(l-z) + \frac{1}{\alpha E_f}\frac{\lambda_1}{\lambda}\omega(\bar{\sigma}+\sigma)(e^{-\lambda z}-e^{-\lambda l}) + \frac{1}{\alpha E_f}\frac{K\lambda_1}{ak_1}\sum_{n=1}^{\infty}B_n\left(\frac{L}{n\pi}\right)\left\{\frac{\lambda_3}{\lambda_1}k_1 - \frac{(\lambda L)^2}{(\lambda L)^2+(n\pi)^2}\right\}\left(\sin\frac{n\pi l}{L} - \sin\frac{n\pi z}{L}\right) + \frac{1}{\alpha E_f}\frac{K\lambda_1}{ak_1}\frac{1}{\lambda}\sum_{n=1}^{\infty}B_n\frac{(\lambda L)^2}{(\lambda L)^2+(n\pi)^2} \times\left(\cos\frac{n\pi l}{L} - \cos\frac{n\pi z}{L} + e^{-\lambda z} - e^{-\lambda l}\right) \quad (37)$$

From Equations 19, 20, 23, and 37, the axial stress distribution $\sigma_f^z(z)$ in the debonded region can be solved numerically. The measured value of the relative displacement Δ at the fiber end $z = 0$ is given by:

$$\Delta = v(0) = \frac{1}{\alpha E_f}\left(\frac{\lambda_1 k_2 - \lambda_2 k_1}{k_1}\sigma - \omega\lambda_1\bar{\sigma} - \lambda_3 q_o + \sigma_o + \frac{\lambda_3 K B_o}{2a}\right)l + \frac{1}{\alpha E_f}\frac{\lambda_1}{\lambda}\omega(\bar{\sigma}+\sigma)(1-e^{-\lambda l}) + \frac{1}{\alpha E_f}\frac{K\lambda_1}{ak_1}\sum_{n=1}^{\infty}B_n\left(\frac{L}{n\pi}\right)\left\{\frac{\lambda_3}{\lambda_1}k_1 - \frac{(\lambda L)^2}{(\lambda L)^2+(n\pi)^2}\right\}\sin\frac{n\pi l}{L} + \frac{1}{\alpha E_f}\frac{K\lambda_1}{ak_1}\frac{1}{\lambda}\sum_{n=1}^{\infty} \times B_n\frac{(\lambda L)^2}{(\lambda L)^2+(n\pi)^2}\left(\cos\frac{n\pi l}{L} - e^{-\lambda l}\right) \quad (38)$$

3.3. Stresses in the bonded region ($l < z < L$)

In the bonded region, no slip condition at the interface [i.e. $u_m^z(a,z) = u_f^z(a,z)$] should be imposed. The shear

stress distribution in the matrix is therefore,

$$\tau_m^{rz}(r,z) = G\gamma_m^{rz}(r,z) = \frac{E_m}{2(1+\nu_m)}\left(\frac{\partial u_m^r(r,z)}{\partial z} + \frac{\partial u_m^z(r,z)}{\partial r}\right) \quad (39)$$

In Equation 39, the radial displacement with respect to the z-direction can be ignored compared to the axial displacement gradient with respect to the r-direction. From Equations 8 and 39

$$\frac{\partial u_m^z(r,z)}{\partial r} = \frac{2(1+\nu_m)}{E_m}\frac{\gamma}{a}\frac{(b^2-r^2)}{r}\tau(z) \quad (40)$$

Integration and rearranging,

$$\tau(z) = \left[u_m^z(b,z) - u_m^z(a,z)\right]\frac{aE_m}{2(1+\nu_m)\gamma} \times \frac{1}{\frac{1}{2}(r^2-b^2) - b^2\ln\frac{r}{b}} \quad (41)$$

Differentiating with respect to z and imposing the no slip condition at the interface results in

$$\frac{d\tau(z)}{dz} = \frac{aE_m}{(1+\nu_m)}\frac{1}{2\gamma b^2\ln\frac{b}{a} - a^2}\left[\varepsilon_m^z(b,z) - \varepsilon_f^z(a,z)\right] \quad (42)$$

The differential equation for axial fiber stress is derived from Equations 1, 2, 5, 7, 12, and 42. Hence, we have

$$\frac{d^2\sigma_f^z(z)}{dz^2} - \eta_1\sigma_f^z(z) = -\eta_1\eta_2\sigma + \eta_1\eta_3\sigma_o + \eta_1\eta_4 q_o \quad (43)$$

where

$$\eta_1 = \frac{2}{(1+\nu_m)}\frac{(\alpha+\gamma) - 2k_1(\alpha\nu_f + \gamma\nu_m)}{2\gamma b^2\ln\frac{b}{a} - a^2} \quad (44)$$

$$\eta_2 = \frac{\gamma(1-2k_1\nu_m)}{(\alpha+\gamma) - 2k_1(\alpha\nu_f + \gamma\nu_m)} \quad (45)$$

$$\eta_3 = \frac{1}{(\alpha+\gamma) - 2k_1(\alpha\nu_f + \gamma\nu_m)} \quad (46)$$

$$\eta_4 = \frac{2(\alpha\nu_f + \gamma\nu_m)}{(\alpha+\gamma) - 2k_1(\alpha\nu_f + \gamma\nu_m)} \quad (47)$$

The resulting equation of the axial stress in the bonded region subjected to the boundary condition $\sigma_f^2(l) = \sigma_f^l$ and $\sigma_f^z(L) = 0$ yields

$$\sigma_f^z(z) = \frac{1}{\sinh\sqrt{\eta_1}(L-l)}\left[\left(\sigma_f^l - \eta_2\sigma + \sigma_r\right)\sinh\sqrt{\eta_1}(L-z) - \left(\eta_2\sigma - \sigma_r\right)\sinh\sqrt{\eta_1}(z-l)\right] + \eta_2\sigma - \sigma_r \quad (48)$$

where $\sigma_f^z(l) = \sigma_f^l$ could be evaluated from Equation 27 using the continuity condition of axial stress and $\sigma_r = \eta_3\sigma_o + \eta_4 q_o$ is the contribution of axial and radial thermal residual stresses.

The corresponding matrix axial stress $\sigma_m^z(z)$ and shear stress in matrix $\tau_m^{rz}(z)$ in the bonded region could be obtained by equilibrium consideration as before

$$\sigma_m^z(z) = [(1-\eta_2)\sigma + \sigma_r]\gamma - \frac{\gamma}{\sinh\sqrt{\eta_1}(L-l)}\left[\left(\sigma_f^l - \eta_2\sigma + \sigma_r\right)\sinh\sqrt{\eta_1}(L-z) - \left(\eta_2\sigma - \sigma_r\right)\sinh\sqrt{\eta_1}(z-l)\right] \quad (49)$$

$$\tau_m^{rz}(r,z) = \frac{\gamma(b^2-r^2)}{2r}\sqrt{\eta_1}\frac{1}{\sinh\sqrt{\eta_1}(L-l)}\left[\left(\sigma_f^l - \eta_2\sigma + \sigma_r\right)\cosh\sqrt{\eta_1}(L-z) + \left(\eta_2\sigma - \sigma_r\right)\cosh\sqrt{\eta_1}(z-l)\right] \quad (50)$$

3.4. Interfacial debonding criterion

The interfacial debonding criterion is derived from the Griffith energy balance equation as the rate change of the total elastic energy, U_t

$$G_c = \frac{\partial U_t}{\partial(2\pi a l)} \quad (51)$$

The total elastic strain energy is obtained from:

$$U_t = \frac{1}{2E_f}\int_0^L\int_0^a\left[\left(\sigma_f^z\right)^2 + \left(\sigma_f^r\right)^2 + \left(\sigma_f^\theta\right)^2 - 2\nu_f\left(\sigma_f^z\sigma_f^r + \sigma_f^z\sigma_f^\theta + \sigma_f^\theta\sigma_f^r\right)\right]2\pi r\,dr\,dz + \frac{1}{2E_m}\int_0^L\int_a^b\left[\left(\sigma_m^z\right)^2 + \left(\sigma_m^r\right)^2 + \left(\sigma_m^\theta\right)^2 - 2\nu_m\left(\sigma_m^z\sigma_m^r + \sigma_m^z\sigma_m^\theta + \sigma_m^\theta\sigma_m^r\right) + 2(1+\nu_m)\left(\tau_m^{rz}\right)^2\right]2\pi r\,dr\,dz \quad (52)$$

The axial and shear components of stresses in the debonded and bonded regions are given in Equations 23, 28, 29, 48, 49, and 50. The radial and circumferential stress components can be solved using the

continuity conditions of stresses and displacements at the interface. Thus,

$$\sigma_f^r = \sigma_f^\theta = q(z) \tag{53}$$

$$\sigma_m^r = \gamma\left(\frac{b^2 - r^2}{r^2}\right)q(z) \tag{54}$$

$$\sigma_m^\theta = -\gamma\left(\frac{b^2 + r^2}{r^2}\right)q(z) \tag{55}$$

where $q(z)$ is interfacial pressure which is different in the debonded and bonded regions. In the debonded region,

$$\begin{aligned} q(z) &= -q_o + k_1\sigma_f^z(z) - k_2\sigma + q_R(z) \\ &= k_1\omega(\bar{\sigma} + \sigma)e^{-\lambda z} - \frac{K}{a}\sum_{n=1}^{\infty}\frac{(\lambda L)^2 B_n}{(\lambda L)^2 + (n\pi)^2} \\ &\quad \times\left(\cos\frac{n\pi z}{L} + \frac{n\pi}{\lambda L}\sin\frac{n\pi z}{L} - e^{-\lambda z}\right) \\ &\quad + \frac{K}{a}\sum_{n=1}^{\infty} B_n\cos\frac{n\pi z}{L} \end{aligned} \tag{56}$$

And in the bonded region,

$$q(z) = \frac{k_1}{\sinh\sqrt{\eta_1}(L-l)}\left[\left(\sigma_f^l - \eta_2\sigma + \sigma_r\right)\sinh\sqrt{\eta_1}(L-z) - \left(\eta_2\sigma - \sigma_r\right)\sinh\sqrt{\eta_1}(z-l)\right] + \eta_5\sigma - \bar{q} \tag{57}$$

where $\eta_5 = k_1\eta_2 - k_2$ and $\bar{q} = k_1\sigma_r + q_o$. The energy balance equation for the fiber-matrix interfacial debonding criterion in Equation 51 becomes:

$$\begin{aligned} 2\pi a G_c = {} & m_1\sigma^2 + m_2(\bar{\sigma} + \sigma)\sigma + m_3(\bar{\sigma} + \sigma)^2 \\ & + m_4\sigma + m_5(\bar{\sigma} + \sigma) + m_6 \end{aligned} \tag{58}$$

where the coefficients m_i are functions of material properties and geometric factors which are derived analytically in Appendix A. Rearrangement of Equation 58 gives the remote stress applied to the fiber for further debond growth. That is,

$$\begin{aligned} \sigma = {} & \frac{1}{2\bar{m}_1}\left[-(\bar{m}_2\bar{\sigma} + \bar{m}_3)\right. \\ & \left. + \sqrt{\bar{m}_4\bar{\sigma}^2 + \bar{m}_5\bar{\sigma} + \bar{m}_6 + 8\pi a\bar{m}_1 G_c}\right] \end{aligned} \tag{59}$$

for which further details of the coefficients $\bar{m}_i$ are given in Appendix B.

4. Results and discussion

To illustrate the effects of interface roughness and thermal residual stresses on the fiber push-out problem, specific analyses were conducted for a steel-epoxy model composite. Its basic physical and mechanical properties are given in Table I. The interface roughness was assumed to have an average wavelength of $0.01L$ and maximum amplitude of $0.005a$ as shown in Fig. 2.

TABLE I Material properties and geometric factors

Fiber	
Young's modulus E_f (GPa)	210
Poisson's ratio ν_f	0.25
Radius a (mm)	2.5
Thermal expansion coefficient α_f^T (10^{-6}/°C)	12
Matrix	
Young's modulus E_m (GPa)	3
Poisson's ratio's ν_m	0.4
Radius b (mm)	10
Thermal expansion coefficient α_m^T (10^{-6}/°C)	65
Interface	
Axial length L (mm)	50
Coefficient of friction μ	0.5
Temperature change ΔT (°C)	−100
Fracture toughness G_c (J/m^2)	20

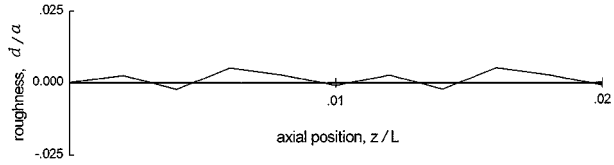

Figure 2 Interface roughness (wavelength: $0.01L = 0.5$ mm, $d_{\max} = 0.005a = 0.0125$ mm).

(Heretofore, all plots in Figs 3–7 correspond to these material parameters and interface roughness dimensions given). An iterative approach was used to calculate the effect of interface roughness represented by the Fourier series coefficient B_n. For a given applied stress, the initial value of the relative displacement function $v(z)$ in Equation 9, when $B_n = 0$, was used to calculate the initial asperities mismatch $\delta(z)$ in Equation 5. Axial fiber stress in Equation 7 and relative displacement $v(z)$ in Equation 9 were then computed after determining the Fourier series coefficients B_n from Equation 6 for an initial value of $\delta(z)$. The iterative process was stopped when the condition of axial fiber stress $\left|\frac{\sigma_f^z(z)_{,i+1} - \sigma_f^z(z)_{,i}}{\sigma_f^z(z)_{,i}}\right| \le 10^{-6}$ was satisfied.

To account for the effect of axial thermal residual stress σ_o on the stress distribution, the variation of the axial fiber stress $\sigma_f^z(z)$ and interfacial shear stress $\tau(z)$ are plotted as a function of the axial distance z in Figs 3 and 4, respectively. Three types of interfacial bond conditions, namely fully bonded, partially debond and fully debonded cases were studied. The debonded length in the partially debonded case was determined from the debonding criterion in Equation 12 for a given applied stress and fiber length. The general trend of the stress distribution was different between the different interfacial bond conditions. In the bonded region (Figs 3a and 4a), the axial fiber stress and the interfacial shear stress decrease rapidly from the loaded end ($z = 0$)

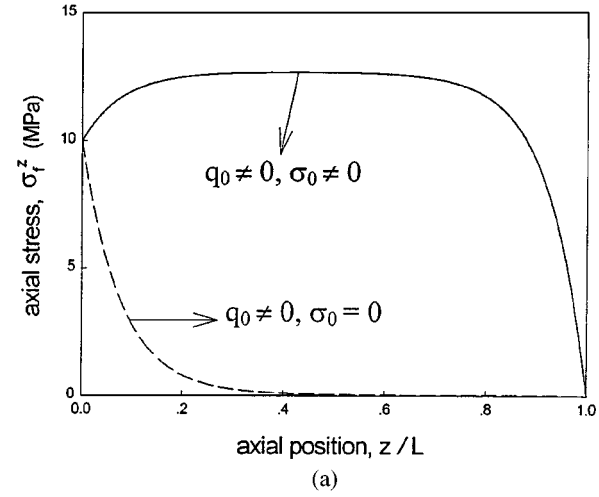

(a)

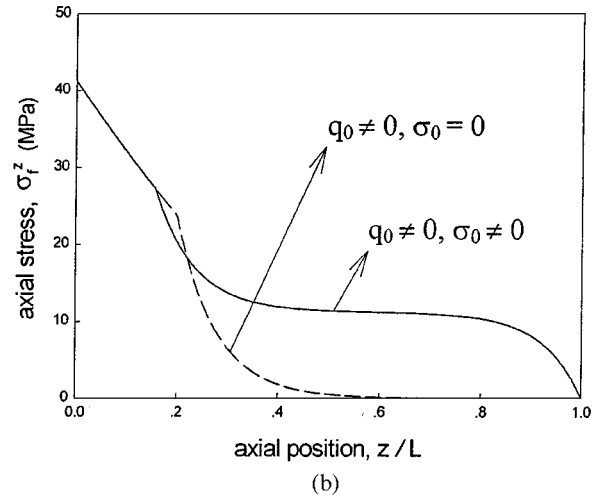

(b)

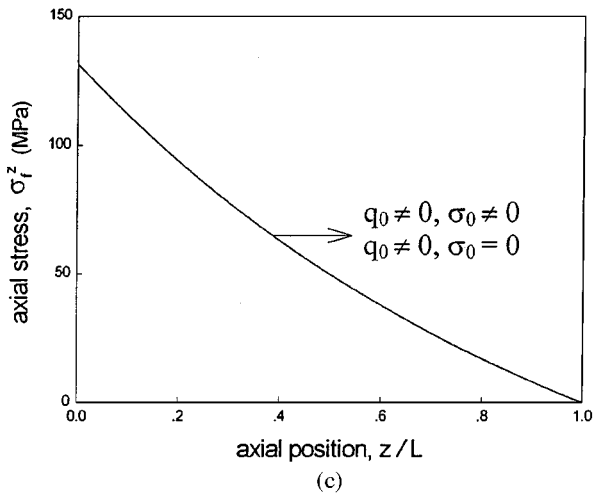

(c)

Figure 3 Axial fiber stress distribution: Effect of thermal residual stress for the cases of (a) fully bonded, (b) partially debonded, and (c) fully debonded.

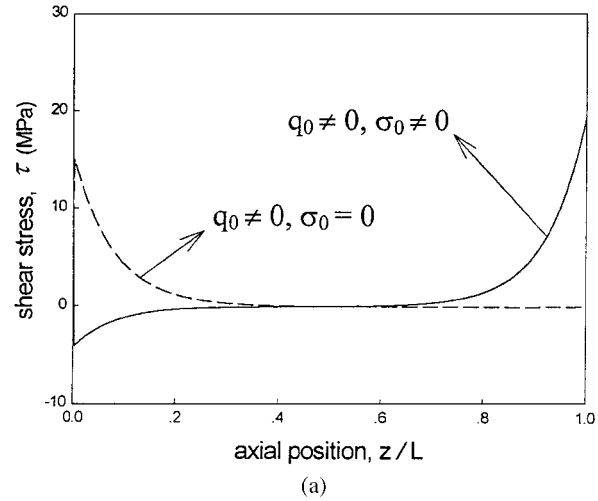

(a)

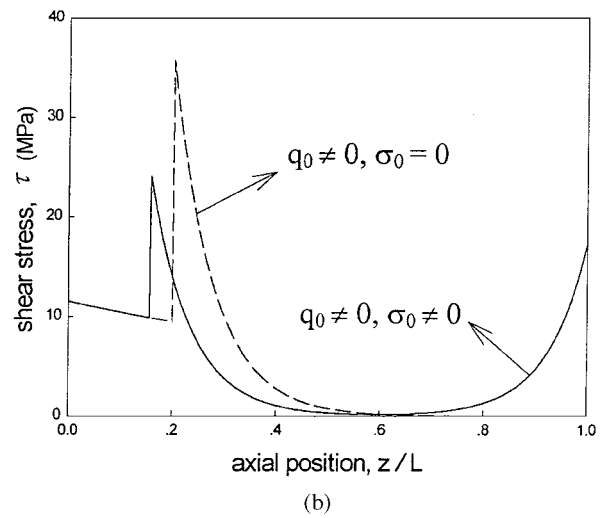

(b)

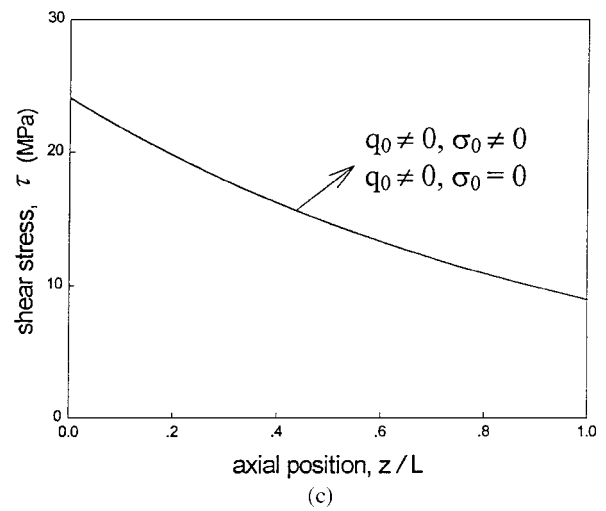

(c)

Figure 4 Interfacial shear stress distribution: Effect of thermal residual stress for the cases of (a) fully bonded, (b) partially debonded, and (c) fully debonded.

towards the bottom end ($z = L$) in the case of zero axial thermal residual stress. The distribution of the axial fiber stress was very much affected by the presence of axial thermal residual stress, which results in a plateau region along the fiber length and diminishes to zero at the free end (Fig. 3a and b). It can be seen that the interfacial shear stress, which plays an important role in interfacial debonding, is also significantly affected by the axial thermal residual stress in the bonded region (Fig. 4a and b). The distribution of the interfacial shear stress in the bonded region which is proportional to the rate change of axial fiber stress as in Equation 2 has two peaks at the loaded end (or debond front) and the bottom free end, Fig. 4a and b, which suggests possible two-way debonding caused by the axial thermal residual stress. Although the peak values of interfacial shear stresses are dependent on the material combination of fiber and matrix, the result has not been observed in earlier studies and is left for future experimental

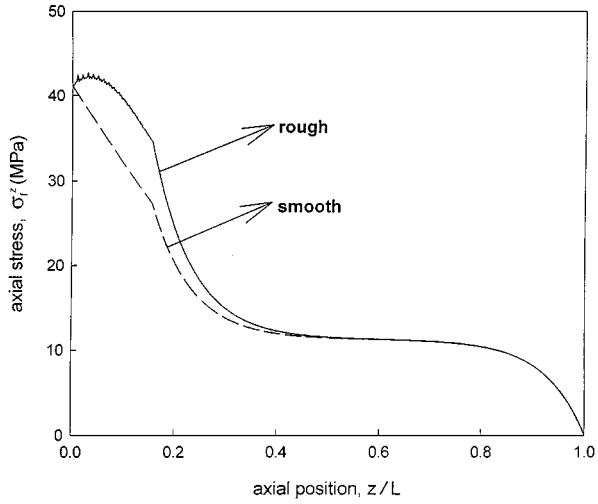

Figure 5 Axial fiber stress distribution showing the effect of interface roughness.

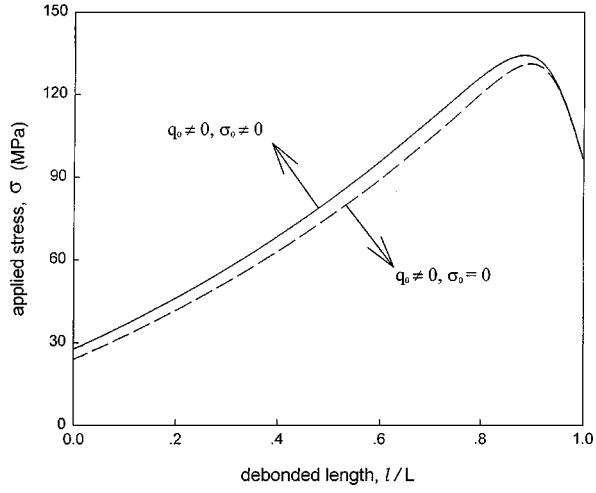

Figure 6 Applied stress required for further debonding: effect of thermal residual stress.

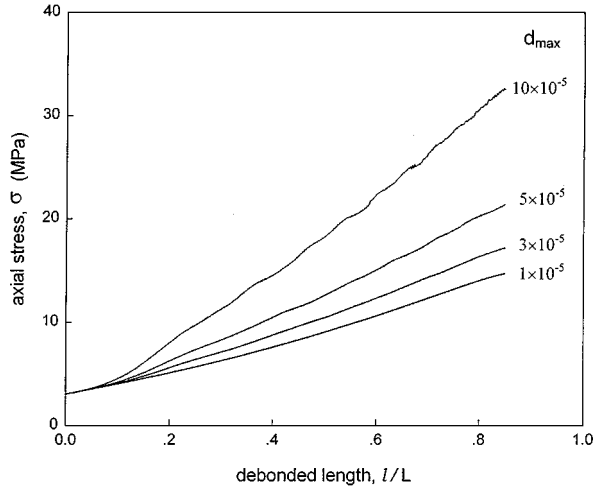

Figure 7 Applied stress required for further debonding showing the effect of interface roughness.

verification. The axial thermal residual stress does not cause any difference in both axial fiber stress and interfacial shear stress in the debonded region (Figs 3c and 4c). The effect of interface roughness on the axial fiber stress distribution is plotted in Fig. 5 for a smooth interface and a rough interface as characterised in Fig. 2. Clearly interface roughness has a significant effect on the axial fiber stress in the debonded region.

The applied stress required for further debonding at the debond length l can be determined from the interfacial debonding criterion of Equation 59. The effect of axial thermal residual stress on interfacial debonding is shown in Fig. 6. Except for the unstable region ($l > 0.85L$), the applied stress required to maintain debonding of the interface is higher in the presence of the axial thermal residual stress. This can be interpreted as a discouragement of interfacial debonding. The effect of interface roughness of different maximum amplitude (d_{max}) but the same average wavelength is also shown in Fig. 7. As expected, the effect of interface roughness on the interfacial debonding behaviour becomes more significant as the amplitude of roughness increases.

5. Conclusions

An improved model considering the effects of interface roughness and thermal residual stresses is presented for the single fiber push-out test. The Fourier representation of the surface roughness and the energetic debond criterion according to Griffith are different to other approaches shown in the literature. The distributions of the axial fiber stress and the interfacial shear stress in the bonded region are significantly affected by the presence of the axial thermal residual stress. The distribution of the interfacial shear stress in the bonded region of a partially debonded interface also suggests a possibility of two-way debonding. Both thermal residual stresses and interface roughness affect the interfacial debonding behavior. It has been shown that larger applied stresses are required for further debonding at given debond lengths.

Appendix A

$$m_1 = \left(1 - 2\eta_2 + 2\eta_2^2\right)\frac{\partial \tilde{F}_1}{\partial l} + \eta_2(1-\eta_2)\frac{\partial \tilde{F}_2}{\partial l} + (1-2\eta_2)\tilde{b}_3\frac{\partial F_3}{\partial l} - b_4 - \eta_5^2 b_5 + \eta_2\eta_5 b_6 + \frac{\pi a^2}{2E_m}\alpha \tag{A1}$$

$$m_2 = \omega e^{-\lambda l}\left[2\lambda(-1+\eta_2)\tilde{F}_1 - \lambda(\eta_2\tilde{F}_2 + \tilde{b}_3 F_3) - k_1\frac{\pi a^2}{E_m}2\alpha\nu_f\right] + \omega(1-e^{-\lambda l}) \times \left[2(-1+\eta_2)\frac{\partial \tilde{F}_1}{\partial l} - \left(\eta_2\frac{\partial \tilde{F}_2}{\partial l} + \tilde{b}_3\frac{\partial F_3}{\partial l}\right) - \frac{\pi a^2}{E_m}\alpha\right] \tag{A2}$$

$$m_3 = \omega^2 e^{-2\lambda l}\left[(1-e^{\lambda l})^2\left(\frac{\partial \tilde{F}_1}{\partial l} + b_2\right) + b_1\lambda^2 + b_5 k_1^2 - (1-e^{\lambda l})(2\lambda\tilde{F}_1 + k_1 b_6)\right] \tag{A3}$$

$$m_4 = -2(1-\eta_2)\left[\frac{\partial \tilde{F}_1}{\partial l}R_n + \tilde{F}_1 Q_n\right] - \eta_2\left[\frac{\partial \tilde{F}_2}{\partial l}R_n + \tilde{F}_2 Q_n\right] - \tilde{b}_3\left[\frac{\partial F_3}{\partial l}R_n + F_3 Q_n\right] + \left[(1-2\eta_2)\frac{\partial \tilde{F}_3}{\partial l} + 2\tilde{b}_3\frac{\partial F_3}{\partial l} - b_3 - \eta_5 b_6\right]\sigma_r + [2\eta_5 b_5 - \eta_2 b_6]\bar{q} - \frac{\pi a^2 \alpha}{E_m}R_n + \frac{\pi a^2}{E_m}(2\alpha\nu_f)(k_1 R_n - P_n) \quad \text{(A4)}$$

$$m_5 = \omega e^{-\lambda l}[2\lambda(\tilde{F}_1 R_n + b_1 Q_n) - \lambda\tilde{F}_3\sigma_r - 2k_1 b_5(k_1 R_n - P_n) + k_1 b_6 R_n] + \omega(1-e^{-\lambda l})\left[2\left(\frac{\partial \tilde{F}_1}{\partial l} + b_2\right)R_n + 2\tilde{F}_1 Q_n - \frac{\partial \tilde{F}_3}{\partial l}\sigma_r - b_6(k_1 R_n - P_n)\right] \quad \text{(A5)}$$

$$m_6 = \left(\frac{\partial \tilde{F}_1}{\partial l} + b_2\right)R_n^2 + 2\tilde{F}_1 R_n Q_n + b_1 Q_n^2 - \left(\frac{\partial \tilde{F}_3}{\partial l}R_n + \tilde{F}_3 Q_n\right)\sigma_r - b_5\bar{q}^2 + b_6\sigma_r\bar{q} + \left(\frac{\partial \tilde{F}_3}{\partial l} + 2\tilde{b}_2\frac{\partial F_3}{\partial l} - b_2\right)\sigma_r^2 + b_5(k_1 R_n - P_n)^2 - b_6(k_1 R_n - P_n)R_n \quad \text{(A6)}$$

where

$$\tilde{F}_1 = F_1 - k_1 b_6 F_4 + k_1^2 b_5 F_4 \quad \text{(A7)}$$

$$\tilde{F}_2 = F_2 + k_1 b_6 F_5 - k_1^2 b_5 F_5 \quad \text{(A8)}$$

$$\tilde{F}_3 = 2\tilde{F}_1 - \tilde{F}_2 + 2\tilde{b}_2 F_3 \quad \text{(A9)}$$

$$F_1 = \frac{1}{2\sqrt{\eta_1}}\left[(b_1\eta_1 - b_2)\frac{\phi}{\sinh^2\phi} + (b_1\eta_1 + b_2)\coth\phi\right] \quad \text{(A10)}$$

$$F_2 = \frac{1}{\sqrt{\eta_1}}\left[(b_1\eta_1 - b_2)\frac{\phi\cosh\phi}{\sinh^2\phi} + (b_1\eta_1 + b_2)\frac{1}{\sinh\phi}\right] \quad \text{(A11)}$$

$$F_3 = \frac{1}{\sqrt{\eta_1}}\frac{(1-\cosh\phi)}{\sinh\phi} \quad \text{(A12)}$$

$$F_4 = \frac{1}{2\sqrt{\eta_1}}\left(\coth\phi - \frac{\phi}{\sinh^2\phi}\right) \quad \text{(A13)}$$

$$F_5 = \frac{1}{\sqrt{\eta_1}}\left(\frac{\phi\cosh\phi}{\sinh^2\phi} - \frac{1}{\sinh\phi}\right) \quad \text{(A14)}$$

$$b_1 = \frac{\pi(1+\nu_m)}{2E_m}\gamma^2\left[b^4\ln\frac{b}{a} - \frac{1}{4}(3b^2 - a^2)(b^2 - a^2)\right] \quad \text{(A15)}$$

$$b_2 = \frac{\pi a^2}{2E_m}(\alpha + \gamma) \quad \text{(A16)}$$

$$b_3 = \frac{\pi a^2}{E_m}[\gamma - (\alpha+\gamma)\eta_2] \quad \text{(A17)}$$

$$b_4 = \frac{\pi a^2}{2E_m}\left[\alpha\eta_2^2 + \gamma(1-\eta_2)^2\right] \quad \text{(A18)}$$

$$b_5 = \frac{\pi a^2}{E_m}[\alpha(1-\nu_f) + (1+2\gamma+\nu_m)] \quad \text{(A19)}$$

$$b_6 = \frac{\pi a^2}{E_m}2(\alpha\nu_f + \gamma\nu_m) \quad \text{(A20)}$$

$$\tilde{b}_2 = b_2 + b_5\frac{\bar{q}}{\sigma_r} - b_6\left(k_1 + \frac{\bar{q}}{\sigma_r}\right) \quad \text{(A21)}$$

$$\tilde{b}_3 = b_3 - 2k_1\eta_5 b_5 + (k_1\eta_2 + \eta_5)b_6 \quad \text{(A22)}$$

$$\phi = \sqrt{\eta_1}(L - l) \quad \text{(A23)}$$

$$P_n = P_n(l) = \frac{K}{a}\sum_{n=1}^{\infty} B_n\cos\frac{n\pi l}{L} \quad \text{(A24)}$$

$$R_n = R_n(l) = \frac{K}{ak_1}\sum_{n=1}^{\infty}\frac{(\lambda L)^2 B_n}{(\lambda L)^2 + (n\pi)^2} \times\left[\cos\frac{n\pi l}{L} + \frac{n\pi}{\lambda L}\sin\frac{n\pi l}{L} - e^{-\lambda l}\right] \quad \text{(A25)}$$

$$Q_n = Q_n(l) = \frac{dR_n(l)}{dl} = \frac{K}{ak_1}\sum_{n=1}^{\infty}\frac{(\lambda L)^2 B_n}{(\lambda L)^2 + (n\pi)^2} \times\left[-\frac{n\pi}{L}\sin\frac{n\pi l}{L} + \frac{n^2\pi^2}{\lambda L^2}\cos\frac{n\pi l}{L} + \lambda e^{-\lambda l}\right] \quad \text{(A26)}$$

Appendix B

$$\bar{m} = m_1 + m_2 + m_3 \quad \text{(A27)}$$

$$\bar{m}_2 = m_2 + 2m_3 \quad \text{(A28)}$$

$$\bar{m}_3 = m_4 + m_5 \quad \text{(A29)}$$

$$\bar{m}_4 = m_2^2 - 4m_1 m_3 \quad \text{(A30)}$$

$$\bar{m}_5 = 2m_4(m_2 + 2m_3) - 2m_5(2m_1 + m_2) \quad \text{(A31)}$$

$$\bar{m}_6 = (m_4 + m_5)^2 - 4m_6(m_1 + m_2 + m_3) \quad \text{(A32)}$$

Acknowledgements

Y-W Mai wishes to thank the Australian Research Council (ARC) for the continuing support of the work on fiber-matrix interfaces. Y. S. Chai is supported by both the ARC International Research Fellowship and the Korea Science & Engineering Foundation (KOSEF), Safety and Structural Integrity Research Center, Republic of Korea.

References

1. Y. C. GAO, Y.-W. MAI and B. COTTERELL, *J. Appl. Math. Phys.* **39** (1988) 550.
2. J. W. HUTCHINSON and H. M. JENSEN, *Mech. Mater.* **9** (1990) 139.
3. L. M. ZHOU, J. K. KIM and Y.-W. MAI, *J. Mater. Sci.* **27** (1992b) 3155.
4. L. M. ZHOU and Y.-W. MAI, *Philos. Mag. Lett.* **68** (1993) 5.
5. *Idem., J. Appl. Math. Phys.* **44** (1993) 769.
6. L. M. ZHOU, J. K. KIM, C. BAILLIE and Y.-W. MAI, *J. Comp. Matls.* **29** (1995) 81.

7. P. D. JERO and R. J. KERANS, *Scr. Metall. Mater*. **24** (1991) 2315.
8. W. C. CARTER, E. P. BUTLER and E. R. FULLER, *ibid*. **25** (1991) 579.
9. R. J. KERANS and T. A. PARTHASARATHY, *J. Amer. Ceram. Soc*. **74** (1991) 1585.
10. T. A. PARTHASARATHY, D. B. MARSHALL and R. J. KERANS, *Acta. Metall. Mater*. **42** (1994) 3773.
11. T. A. PARTHASARATHY, D. R. BARLAGE, P. D. JERO and R. J. KERANS, *J. Amer. Ceram. Soc*. **77** (1994) 3232.
12. T. J. MACKIN, J. YANG and P. D. WARREN, *ibid*. **75** (1992) 3358.
13. T. J. MACKIN, P. D. WARREN and A. G. EVANS, *Acta. Metall. Mater*. **40** (1992) 1251.
14. H. Y. LIU, L. M. ZHOU and Y.-W. MAI, *Philos. Mag*. **70** (1994) 359.
15. *Idem*., *J. Amer. Ceram. Soc*. **78** (1995) 560.
16. S. STUPKIEWICZ, *Mech. Mater*. **22** (1996) 65.
17. T. A. PARTHASARATHY and R. J. KERANS, *J. Amer. Ceram. Soc*. **80** (1997) 2043.
18. C. K. Y. LEUNG and V. C. LI, *Composites* **21** (1990) 305.
19. J. K. KIM and Y.-W. MAI, "Engineered Interfaces in Fiber Reinforced Composites" (Elsevier, Oxford, 1998) p. 401.

Received 22 September 1998
and accepted 6 September 2000